JAAS

ROYAL SOCIETY OF CHEMISTRY

TECHNICAL NOTE

View Article Online
View Journal | View Issue

Cite this: J. Anal. At. Spectrom., 2026, 41, 78

Electrochemical wet-cell fabrication for *in situ* soft X-ray hyperspectral imaging of real-life ORR electrocatalysts

Benedetto Bozzini, *[a] Alessandro Alleva, [a] Maria Eugenia Fortes Brollo,[bc] Regina Ciancio,[cb] Simone Dal Zilio, [b] George Kourousias, [d] Francesco Nespoli,[a] Paolo Ronchese[cb] and Alessandra Gianoncelli [d]

Over the past decade, electrochemical *in situ* imaging and spectral imaging with soft X-ray probes have evolved from a high-risk pioneering challenge to established techniques that now receive substantial beamtime at synchrotron imaging beamlines. Despite a growing body of literature and near-commercial solutions, setting up wet electrochemical cells for these experiments remains challenging and non-routine. Moreover, most published studies revolve around *bona fide* model materials or environments rather than systems mimicking real *in operando* conditions. Thus, the concrete impact of these potentially extraordinarily informative approaches remains questionable outside the community of method specialists. In this context, this study aims to lay the foundation for the development of real-life electrocatalysts under electrochemical control. Since these materials are typically fabricated in powder form, their transfer and fixation onto the electrode system of the *in situ* cell, simultaneously ensuring an appropriate optical density for a high signal-to-noise ratio and maintaining electrochemical activity, remains an open question. The approach is general in nature, but, in this study, we specifically concentrate on α-MnO_2 nanowires, a widely employed oxygen reduction reaction (ORR) electrocatalyst for alkaline metal-air batteries, and describe: (i) the methodology for particle attachment and electrochemical activity assessment; (ii) the fabrication of electrochemical wet cells compatible with these materials; and (iii) the preliminary feasibility of spectral scanning transmission X-ray microscopy (STXM) results at the Mn L-edge.

Received 21st August 2025
Accepted 6th November 2025

DOI: 10.1039/d5ja00322a

rsc.li/jaas

1. Introduction

Understanding the electrochemical processes in energy storage and conversion systems relies on detailed knowledge of the active layer (AL) architecture. Essentially, electrochemical energy devices owe their functionality to ALs that incorporate the electrocatalyst, electronic conductivity additives and a binder within a porous structure of appropriate porosity and tortuosity.[1,2] Each component crucially contributes to the overall electrode performance, while their degradation pathways control the operating mode and lifetime of the system. To date, electrode fabrication protocols have relied on trial and error approaches, where the outcomes from the tests on operational functionality are interpreted in terms of phenomenological electrokinetic and material evolution models. Access to molecular-level observables is essential for well-substantiated advancements. To this end, soft X-ray scanning transmission X-ray microscopy (STXM) hyperspectral imaging offers a powerful tool for studying electrocatalyst components, providing space-dependent electronic-structure information. The combination of this technique with computational modelling can reveal the impact of architecture on electrochemical activity. Research in this field has been very active over the last decade, achieving a solid foundation for wet cell design and data acquisition and processing, but the implementation of realistic materials remains a challenge.

Specifically, numerous studies have reported methodological work on cell development and operation,[3,4] with specific reference to electrocatalysis-related experiments.[5,6] *Ex situ* spectral STXM studies have been conducted on different model materials related to electrocatalysts.[7–11] Methodologically, similar studies have been published on a slightly different topic of battery materials.[12,13] The details of these experiments and systems are reported in Section S1 of the SI. Recently, *ex situ* spectral STXM and spectro-ptychography studies have been carried out using real-life electrocatalysts.[2,14–16] For details, refer to Section S2 of the SI. As far as *in situ* and *in operando* spectral STXM electrocatalysis is concerned, all published studies revolve around model materials.[6,8,17–24] In addition, *in situ*

[a]Department of Energy, Politecnico di Milano, Via Lambruschini 4, 20156 Milano, Italy. E-mail: benedetto.bozzini@polimi.it
[b]CNR-IOM, Area Science Park Basovizza, SS 14 km 163.5, 34139 Trieste, Italy
[c]Area Science Park, Padriciano 99, 34139 Trieste, Italy
[d]Elettra-Sincrotrone Trieste S.C.p.A., SS 14, km 163.5 in Area Science Park, 34149 Trieste-Basovizza, Italy

spectro-ptychography of model materials has been reported.[22–24] It is also worth recalling here methodologically cognate work performed with granular battery materials.[25–27] A brief description of the types of studies published in this field can be found in Sections S3 and S4 of the SI. A comment on the exact meaning of *in situ* and in *operando* is reported herein. Finally, it is worth mentioning here that *in situ* differential soft X-ray radiography, though without spectral information, has been proposed for electrocatalyst studies.[28,29] Further information can be found in Section S5 of the SI. We can thus conclude that, apart from the *ex situ* and *post mortem* studies with electrocatalysts disassembled from real battery GDEs of,[2,14] no spectral STXM work has addressed real-life electrocatalysts synthesized using state-of-the-art powder-production methods and transferred to an electrochemical cell. Moreover, no *in situ* STXM studies on ORR have been conducted in the literature.

Owing to the similarity of wet-cell requirements for *in situ* STXM and TEM cells, as well as their actual intermodality capability, it is worth commenting on cognate work carried out by *in situ* TEM with close-to-real electrocatalysts, synthesized in powder form and transferred to the wet cell to form a membrane-supported electrode system (MSES).[30–36] The key message is that limited factual information is available on the electron-transfer capabilities between the current-feeder and the electrocatalyst particles, and it remains unclear whether the reported electrochemical response originates from the electrocatalyst or from the current-collectors exposed to the electrolyte. Brief details of the individual systems addressed are reported in Section S6 of the SI.

In this context, this study presents a simple and previously undocumented approach to carry out *in situ* spectral STXM measurements in wet cells, with electrochemical control of real-life electrocatalyst particles transferred to a three-electrode system. Specifically, our focus is on ensuring (i) particle attachment to the current-collector, (ii) charge-transfer from the current-collector to the particle, and (iii) localization of electrochemical activity at the electrocatalyst, rather than at the current-collector surface. As a representative system, we consider α-MnO_2 NWs, an efficient ORR electrocatalyst for alkaline aqueous metal-air batteries.[37] Previous *ex situ* studies by our group on GDE ageing have shown different types of morphochemical and crystallographic evolutions of α-MnO_2 NWs[38,39] and NW bundles.[2,14] In order to deepen the understanding of the correlation between the morphochemical evolution of the electrocatalyst and the degradation of ORR performance, we aim to carry out *in situ* spectral STXM studies of pure α-MnO_2 NW bundles at the Mn L-edge. This study describes the first methodological step in this direction. We are convinced that explicit reporting of this non-trivial achievement could be helpful for the community to develop similar approaches.

2. Experimental

In this section, in addition to the details of the analytical methods and instrumentation employed in this research, we report details on the preparation of electrocatalyst materials. The manipulation of electrocatalysts in view of their transfer to the wet cell is an integral part of the results of this technical note, as reported in Section 3. Similarly, the cell fabrication details are the original solutions that we have presented in the Results and Discussion section.

2.1 Synthesis of α-MnO_2 nanowires

ORR electrocatalytic α-MnO_2 NWs were synthesized using a microwave-assisted hydrothermal method. 0.314 g K_2SO_4 (Sigma-Aldrich Chemie GmbH), 0.486 g $K_2S_2O_8$ (Sigma-Aldrich PTE Ltd) and 0.203 g $MnSO_4 \cdot H_2O$ (Merck, ACS, Reag. Pg Eur) were dissolved in 10 mL of Millipore water (Milli-Q® water, TKA, water conductivity of 0.055 μS cm^{-1}). The solution was transferred to a 30 mL quartz reaction vial (G30 reaction vessel) equipped with a magnetic stirring bar and then sealed with a PTFE gasket. The mixture was held at 200 °C for 30 min in a microwave reactor (Monowave 400, Anton Paar GmbH), delivering the maximum power to maintain the prefixed temperature. The stirring rate was set to 600 rpm. These conditions were empirically determined to ensure the formation of pure α-MnO_2, as assessed using XRD and Raman spectroscopy.[2] The collected mixture was washed with 200 mL of ethanol and deionized using a Buchner filter. The washing procedure was repeated 5 times, and after each filtration step, the pH of the filtrate was checked to ensure the effectiveness of the removal of the acidic aqueous reaction matrix. The washed synthesized product was dried overnight at 45 °C in air in a Thermo Scientific VT 6060 M oven. Finally, the powder was hand-ground in an agate mortar for 15 min to pulverize the solid compounds. Disaggregation of the millimeter-sized clumps resulting from the drying process down to micrometric aggregates and preservation of the NW structure after grinding were assessed by SEM and TEM, respectively (Panels A and B–F of Fig. S1 of the SI).

2.2 Spectral scanning transmission X-ray microscopy

STXM at the Mn L-edge was conducted at the TwinMic beamline[40] of the Elettra Trieste Synchrotron facility. A zone plate (ZP) diffractive focusing lens forms a microprobe on the sample plane, and the specimen is raster-scanned across it on a pixel-by-pixel basis. A fast-readout CCD camera collects the X-ray photons transmitted by the sample point by point in the raster scan, producing absorption and differential phase contrast images[41] (Fig. 1A). For the experiments described in this work, a 600 μm Au multilayer diameter ZP with 50 nm outermost zone width was used, with around 1.8 mm distance between the OSA and sample (Fig. 1B). For the present experiment, stacks of images were acquired across the Mn L2,3-edges located at 638.7 and 649.9 eV. The dwell time was set to 80 ms per pixel. To jointly optimize energy resolution in the ranges that are crucial for chemical-state assessment and experimental time, a step of 1 eV was chosen (i) in the pre-edge range from 635 to 636 eV, (ii) in the edge range from 636 to 647 eV and (iii) in the post-edge zone from 652 to 659 eV. The range around the first edge from 636 to 642 eV was scanned with a higher resolution in steps of 0.25 eV, while in the less diagnostic range of

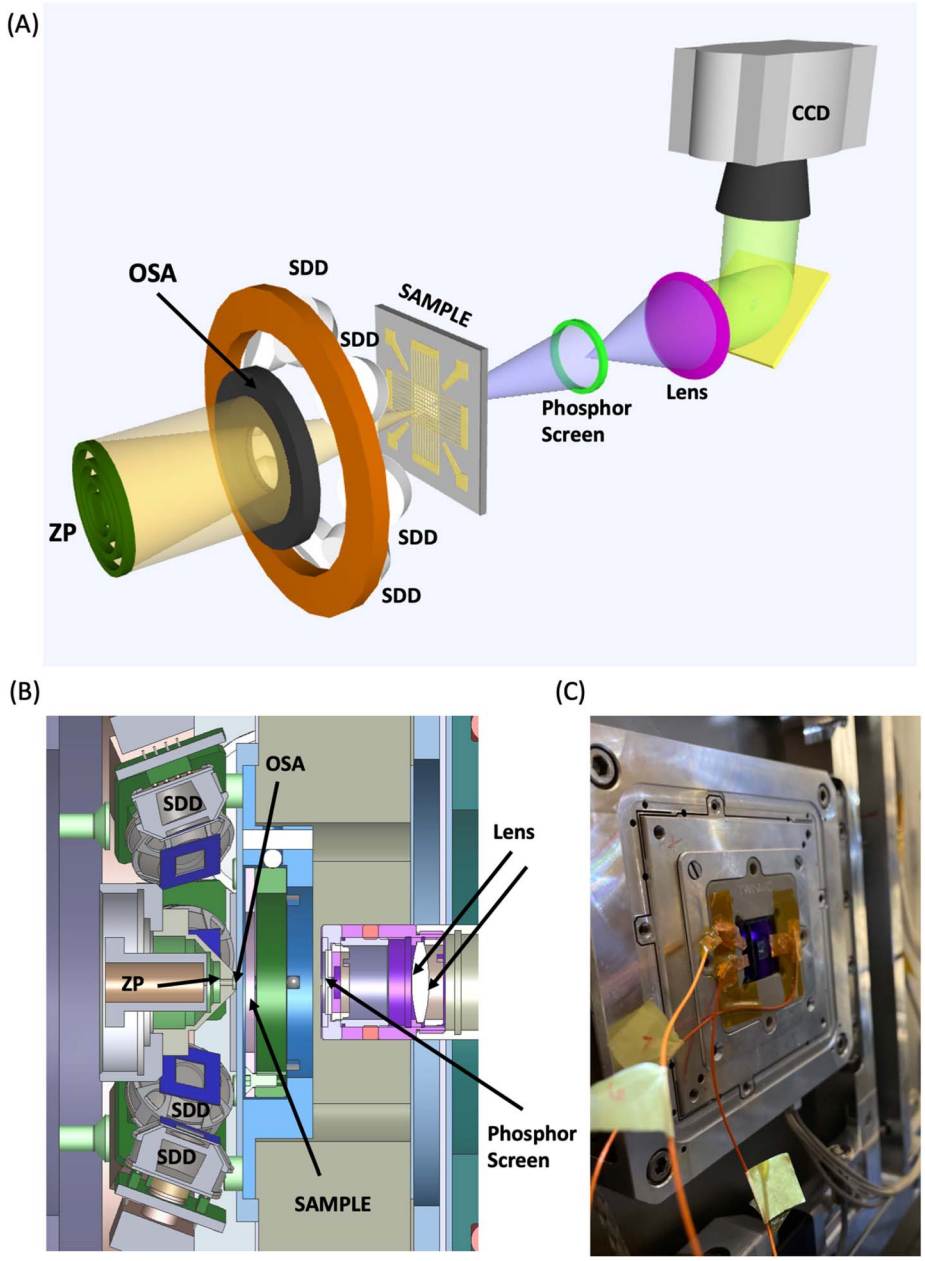

Fig. 1 (A) Schematic of the whole STXM experimental set-up. (B) Cross-section of the TwinMic experimental chamber in the region around the sample, depicting the position of the zone plate (ZP), order sorting aperture (OSA), sample, XRF detectors (SDD) and X-ray to visible light converting system (phosphor screen and lens). (C) Picture of the sealed and bonded wet cell mounted on the TwinMic sample stage, with the chamber open and in air.

647–652 eV, the energy step was set to 0.5 eV. At each energy step, the zone-plate-based diffractive optics were automatically refocused on the samples, delivering a probe size of around 250 nm in diameter. Appropriate post-processing and alignment of the collected stacks of images enabled the extraction of the XAS spectra on a pixel-by-pixel basis.

2.3 Electrochemical measurements

Electrochemical measurements were performed using a VersaSTAT 3 potentiostat. Specifically, a series of 10 cyclic voltammetry (CV) scans at 5 mV s^{-1} were applied in either air-saturated or de-aerated 0.1 M KOH electrolyte, a classical ambient for ORR electroanalysis (*e.g.* 2 and references therein). The reference electrode (RE) was Hg/HgO, and the counter electrode (CE) was a Pt wire of area *ca.* 1.5 cm^2. Cycling was carried out in the potential range −0.45–0.40 V *vs.* Hg/HgO, representative of ORR electrocatalysis with some degree of cathodic stress, resulting in cyclical Mn(IV)/Mn(II) reduction/oxidation, which enables the assessment of active material transformations. Electrochemical tests were carried out in a hanging-meniscus configuration, with the functionalized membrane exclusively in contact with the electrolyte.

As detailed in Subsection 3.2, in the wet cell, an Au quasi-RE was used; we calibrated the Au quasi-RE potential scale with respect to the Hg/HgO one, with both open-circuit potential (OCP) and CV measurements at a polycrystalline Au electrode in Ar-deaerated 0.1 M KOH. A remarkably stable potential difference of 25 mV was observed, indicating that the Au pseudo-RE was fully adequate for electroanalytical measurements in the relevant system.

2.4 Scanning electron microscopy (SEM) and energy-dispersive X-ray spectrometry EDX analysis

Morphological analyses of the samples were conducted using a field emission scanning electron microscope (FE-SEM: Zeiss SUPRA 40, Jena, Germany) operating under high vacuum conditions at room temperature and equipped with an EDX spectrometer. Imaging was performed at an accelerating voltage of 20 kV.

2.5 Transmission electron microscopy (TEM)

TEM imaging of the α-MnO_2 NWs is performed by means of a JEOL JEM 2010F Schottky FEG Transmission Electron Microscope operating at 200 kV. The images are collected by employing a TVIPS TemCam-F216 camera equipped with a 2k x 2k CMOS sensor and controlled by EM-Menu 4 software. The samples for TEM analyses were prepared as follows: α-MnO_2 NWs were dispersed in isopropanol and sonicated. The so-obtained suspension was then drop-cast onto a standard 3 mm carbon-coated copper grid.

3. Results and discussion

The workflow of this research is structured around four key conceptual steps: (i) establishing protocols for the transfer and attachment of α-MnO_2 NW electrocatalysts onto the MSES consisting of a soft-X-ray transparent membrane, equipped with a current corrector system designed to operate as a working electrode (WE); (ii) assessment of the electrochemical activity of NWs and of the localization of electrochemical reactivity on the electrocatalyst rather than on the current-collector; (iii) microfabrication of the electrochemical wet cell and transfer of the electrocatalyst to the electrode system; and (iv) STXM testing of the wet cell. Research regarding Points (i) and (ii) is reported in Subsection 3.1, Step (iii) is the object of Subsection 3.2, and the spectral STXM demonstration is reported in Subsection 3.3.

3.1 Preparation and testing of the α-MnO_2 NW-functionalized membrane-supported electrode system (FMSES)

For operational flexibility and convenience, the protocol for MSES functionalization and testing was developed on Au TEM grids with a C film support. Au and C were chosen as current-collector materials owing to their minimal electrocatalytic activity, which favours the localization of electrochemical activity at the α-MnO_2 NWs. The particles attached to the C coating can be imaged by soft X-ray in transmission. The outcomes of the protocol for particle attachment on TEM grids were then transferred to the functionalized Si_3N_4 membranes of the lithographed wet cell (Subsection 3.2). Two approaches were explored to achieve NW adhesion and ensure charge-transfer from the current-collector to the NWs: (i) covering the NWs, previously cast on the TEM grid, with a pinhole-perforated Au film and (ii) relying on charge-transfer bonding and London dispersion forces, which, in principle, can be stabilized by the presence of the electrolyte. A molecular-level investigation of these mechanisms is beyond the scope of the present work, which focuses solely on demonstrating the physical feasibility of the process.

α-MnO_2-FMSES samples were prepared by depositing the NWs onto Au TEM with C film support grids (Agar Scientific Square Pattern 100 Mesh TEM Support Grids). The deposition was performed *via* drop-casting of a suspension of rods in isopropanol. The suspension was prepared as follows. First, a concentrated suspension was prepared by sonicating 20 mg of α-MnO_2 in 10 mL of isopropanol for 2 min at 10 W using a tip sonicator (UP200 St, Ultrasonic processor, Hielscher Ultrasonics GmbH). The final suspension, at a concentration of 0.15 mg mL^{-1}, was obtained by sonicating 1 mL of the concentrated solution in 12.5 mL of isopropanol under the same conditions. The final suspension was sonicated for 5 min in an ultrasonic bath immediately prior to casting. Drop-casting was carried out by placing the TEM grid on an absorbent paper and depositing a 2 μL drop using a micropipette, after which the sample was air-dried. To ease manipulation and electrical contact, the functionalized TEM grid was glued to a piece of carbon paper, and the contact resistance was verified to be negligible *via* impedance spectrometry.

The mechanical adhesion of the NW bundles was assessed by SEM imaging before and after immersion in the 0.1 M KOH electrolyte (Panels F–I of Fig. S1 of the SI), confirming firm adherence to the substrate in both conditions.

In order to ensure electrical contact to the NW bundles, in the first version of the FMSES, an Au front-contact was applied in order to embed the electrocatalyst into an electronically conducting layer that, on the one hand, could secure adhesion to the support and, on the other hand, could be electrochemically inert in the potential range of interest for α-MnO_2 electrocatalyzed ORR. Front-contact fabrication was implemented by masking the FMSES with an Al mesh and evaporating Au to a nominal thickness of 5 nm (mask details shown in Fig. S2A of the SI). EDX mapping data, reported in Fig. S3 of the SI, showed that the Au distribution behind the Al grids provided effective porosity, ensuring both frontal contact with the NW bundles and exposure to the electrolyte. The voltammetric response of the FMSES (Fig. S2B of the SI, red plot) clearly indicates highly reversible ORR electroactivity and stability of the electrocatalyst. For reference, we also report the CV response of the electrode without NW functionalization. The onset potential is characteristic of α-MnO_2, and a contribution to the electrochemical response from the Au current-collector can be excluded. The slight morphological changes observed in the SEM images of Panels C and D of Fig. S2 of the SI align with the expected formation of ORR-induced MnO_2 films,[2,39]

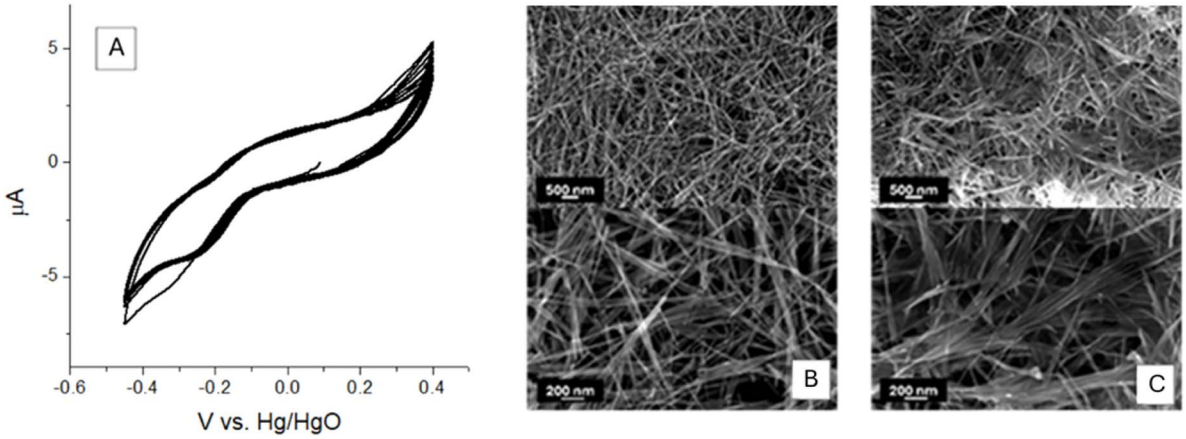

Fig. 2 Functionalized membrane-supported electrode system (FMSES) without front-contact. (A) Cyclic voltammetry at the NW-functionalized TEM grid in de-oxygenated 0.1 M KOH. (B and C) Morphology of the same region of the TEM-grid-supported NWs with the pinhole-perforated Au overlayer (B) before and after (C) the electrochemical test of (A).

confirming that the NW bundles were actually involved in the electrochemical process and remained adhered to the support.

Since, in principle, London dispersion forces can ensure both mechanical adhesion and electronic contact between the NW bundles and the substrate, in order to simplify FMSES fabrication, we also examined the option of casting the NW bundles without the application of a pinhole-perforated Au front-contact. To rigorously assess the electrochemical activity of MnO_2, we excluded the ORR by deaerating the solution by bubbling Ar for 30 min and then keeping an Ar covering atmosphere during the measurement to ensure that the observed electrochemical signal corresponded only to the redox of manganese. Fig. 2A demonstrates the characteristic Mn(IV) → Mn(III) reduction feature[39] around −0.2 V *vs.* Hg/HgO and its oxidation counterpart at *ca.* 0.2 V. Representative SEM images of the FMSES before and after electrochemical testing (Panels B and C of Fig. 2) showed the expected morphological changes, which indicates the oxidation-reduction stress of α-MnO_2 NWs,[14] confirming their electrochemical activity. As a result of this assessment, the Au front contact proved unnecessary and was not adopted in the wet cell fabrication process, as described in the next subsection.

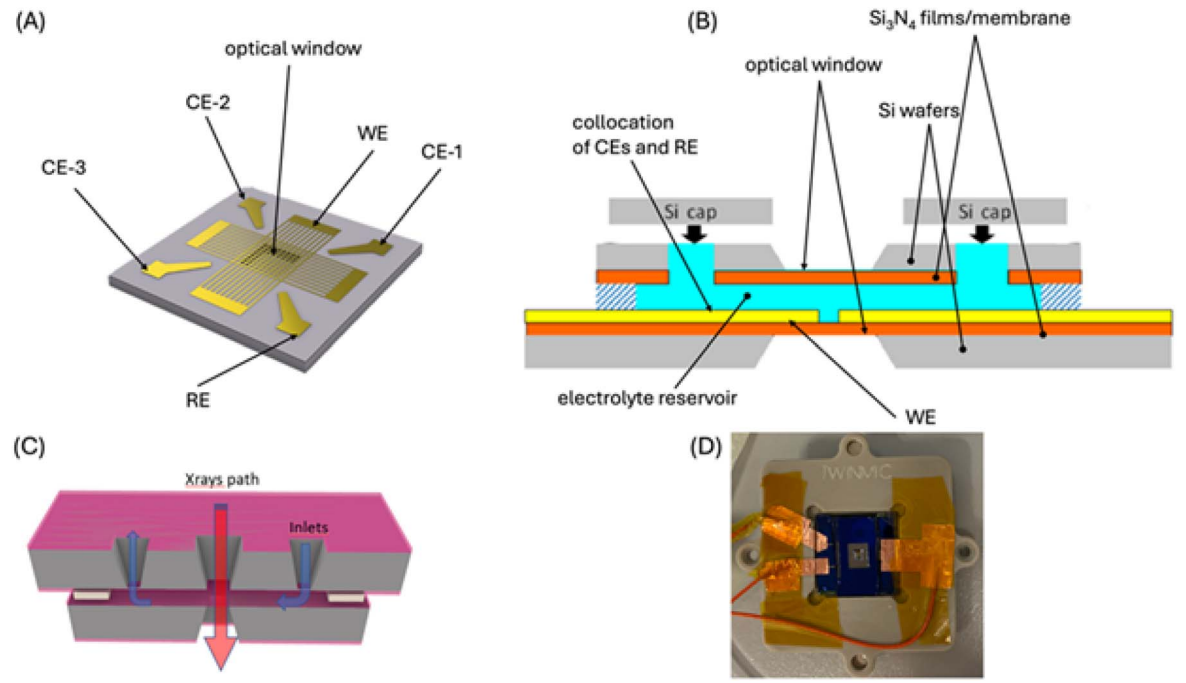

Fig. 3 Schematic of the wet cell. (A) The Si_3N_4 membrane carrying the whole Au electrode system, consisting of working electrode (WE), reference electrode (RE) and three redundant counter electrodes (CE), fabricated by electron lithography. (B and C) Cross sections of the cell with the indication of the collocation of the electrodes (B), electrolyte (B and C) and X-ray path (C). (D) The sealed and bonded wet cells.

3.2 Design and fabrication of the wet cell

The design of the wet cell builds on a solution previously developed in our group, as detailed in 6. The key modification with respect to this concept concerns the Au electrode system, which was redesigned to accommodate the externally applied NW bundles, rather than to support the electrodeposition process, as in our previous studies. Specifically, the whole electrode system, comprising WE, RE, and CE (Fig. 3A), was fabricated onto a 50 nm thick Si_3N_4 optical window. The electrode system consisted of 30 nm thick Au films grown by electron-beam lithography onto Si_3N_4 with a 5 nm thick Ti adhesion layer. The electrocatalyst particles are drop cast on this electrode-functionalized membrane according to the procedure illustrated in the previous section. Only the WE, in the form of an Au grid, is in the field of view, while the Au quasi-RE and the three CEs (one used for the actual measurement and two spare ones) are placed in the electrolyte reservoir outside the field of view (Fig. 3B).

The fabrication process (Fig. 4) started with a silicon wafer (thickness: 500 μm) coated with a 100 nm-thick silicon nitride (Si_3N_4) layer grown by low-pressure chemical vapor deposition (LPCVD). Fluidic inlets and central membrane windows were defined using standard optical photolithography, followed by dry etching in a reactive ion etching (RIE) system with an SF_6/O_2 gas mixture to selectively remove the exposed Si_3N_4. Membrane openings, 1 mm × 1 mm I size, were then formed *via* anisotropic wet etching in 33 wt% KOH solution at 75 °C. On the chip containing the fluidic inlets, a thin film of negative photoresist (SU-8 3005, thickness: 500 nm) was deposited by spin-coating and photolithographically patterned to create a frame serving both as a spacer and a microfluidic channel structure. On the upper chip, a metallic grid was patterned within the central window using electron beam lithography. A 200 nm-thick PMMA layer was spin-coated and exposed using electron beam lithography. After development, the sample was treated with O_2 plasma to enhance metal adhesion. A bilayer of 5 nm titanium (as an adhesion layer) and 30 nm gold was then deposited by electron-beam evaporation. The lift-off process was carried out in warm acetone, resulting in a final metal grid structure, as shown in the figure. Finally, the two chips were aligned using the central windows and mechanically pressed together using a pneumatic press. Under compression, a UV-curable adhesive resin was applied around the perimeter of the smaller (upper) chip and exposed to ultraviolet light to initiate crosslinking, thereby sealing the microfluidic cell. Before closing the cell, the WE, represented by the chips with one optical window depicted in Fig. 4, was functionalized with α-MnO_2 NW bundles without front-contact using the method described in Subsection 3.1.

3.3 Wet cell testing and proof-of-concept spectral STXM test

After building the wet cell (Fig. 3B) around the FMSES (Fig. 3A), the system was filled with 0.1 M KOH aqueous solution from the inlet, and both the inlet and outlet were capped by a piece of Si chip sealed with nail polish. Finally, the WE, CE and RE pads were bonded using Ag conducting glue, and the cables were protected with Kapton tape to prevent short circuits. The sealed and bonded wet cells mounted on the TwinMic sample holder are shown in Panels D and E of Fig. 3.

The cell was held under open-circuit potential (OCP) conditions, and a stack of images was acquired by scanning the energy across the Mn L-edge. Representative absorption images recorded below (640 eV) and above (645 eV) the absorption edge are reported in Panels A and B of Fig. 5. The absorption spectrum, obtained by integrating the optical density over the regions indicated by the yellow lines in Panels A and B, is reported in Fig. 5c. This spectrum fully matches the spectra and spectral STXM images of pristine α-MnO_2 recorded *ex situ* at the same beamline.[2,14] These results, though suboptimal in terms of signal-to-noise ratio and limited to OCP conditions for reasons of available beamtime, clearly demonstrate the hyperspectral capability with respect to α-MnO_2 immobilized in the wet cell.

To further broaden the analytical potential of this approach, we envision an integrated *in situ* correlative workflow

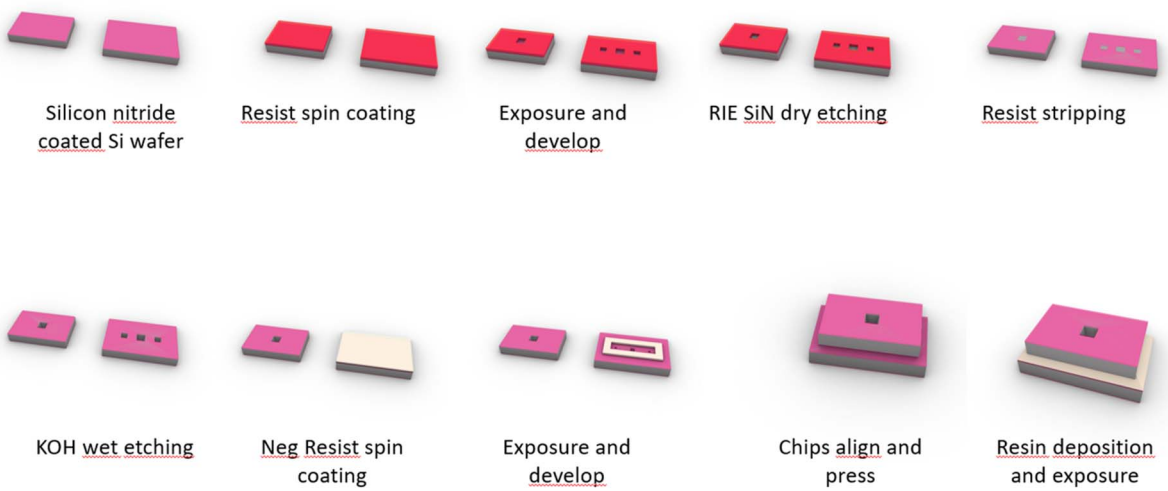

Fig. 4 Schematic of the wet cell fabrication workflow.

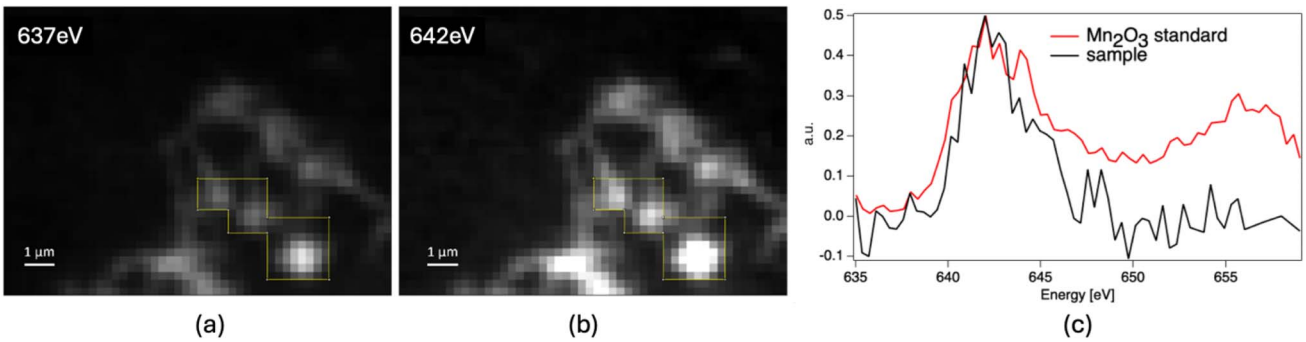

Fig. 5 Hyperspectral soft X-ray absorption microscopy of a pristine α-MnO_2 sample in a wet cell at OCP. (a and b) Absorption images recorded at the indicated beam energies. (c) Spectrum measured at the Mn L-edge by averaging the region of the sample outlined in the panels (a) and (b), plotted together with the spectrum obtained on a grain of a Mn_2O_3 reference standard used for comparison.

combining soft X-ray STXM with transmission electron microscopy (TEM). The structural, crystallographic, and high-resolution morphological information accessible by *in situ* TEM could complement the chemical-state sensitivity of STXM, particularly in tracking redox-driven transformations and degradation pathways in electrocatalyst nanoparticles. Given the converging requirements in wet-cell microfabrication for both techniques (*e.g.* membrane-supported electrodes, microfluidic integration, and electron-transparent windows), developing a dual-compatible platform is a realistic prospect. Although correlative STXM-TEM workflows under electrochemical control are not yet fully established, early-stage demonstrations of electrochemical TEM with drop-cast electrocatalysts suggest a strong foundation upon which such a multimodal methodology could be built. This approach, which is part of a separate study now in progress, would enable spatially correlated, time-resolved insights into electrocatalyst evolution, substantially enhancing our understanding of functional degradation mechanisms.

4. Conclusions

This study establishes a methodological framework for the fabrication and testing of electrochemical wet cells tailored to the *in situ* soft X-ray hyperspectral imaging of realistic electrocatalysts. Specifically, we focused on α-MnO_2 nanowires (NWs), a promising ORR electrocatalyst for alkaline metal–air batteries, and successfully demonstrated their integration into membrane-supported electrode systems (MSESs) while ensuring the selective electrochemical activity of the electrocatalyst. A key aspect of this work was designing an electrode system to exclude electrochemical interference from the current-collector. By addressing the key challenges of particle adhesion and charge transfer at the current-collector interface, we devised a practical protocol for electrocatalyst incorporation that ensures functional electrochemical behavior while preserving the structural integrity and real-life ambient of the NWs. The fabrication process, involving drop-casting of NWs and optional pinhole-perforated Au front-contact deposition, proved effective in establishing robust adhesion and stable redox cycling, as evidenced by cyclic voltammetry tests and morphological SEM analyses.

The development and assembly of the electrochemical wet cell, compatible with synchrotron-based scanning transmission X-ray microscopy (STXM) environments, represents a significant step forward in the investigation of electrocatalyst behavior under realistic operational conditions. The successful acquisition of hyperspectral data across the Mn L-edge under open-circuit potential conditions validates both the electrical and mechanical robustness of the cell, confirming that the feasibility of *in situ* measurements can provide unique insight into the degradation mechanisms and redox transformations of electrocatalysts under practically relevant conditions. Adapting this wet cell design for complementary imaging or spectroscopic techniques could provide a more comprehensive understanding of electrocatalyst behavior. Beyond α-MnO_2 NWs, this methodology holds the potential for broader applications to other electrocatalysts, contributing to the development of efficient and sustainable energy technologies.

Author contributions

Benedetto Bozzini – Conceptualization, data curation, formal analysis, funding acquisition, investigation, methodology, project administration, resources, software, supervision, validation, visualization, writing – original draft. Alessandro Alleva – Data curation, formal analysis, investigation, methodology, validation, visualization, writing – review & editing. Maria Brollo – Data curation, investigation, methodology, validation, visualization, writing – review & editing. Regina Ciancio – Conceptualization, formal analysis, investigation, methodology, resources, validation, visualization, writing – original draft. Simone Dal Zilio – Investigation, methodology, validation, visualization, writing – original draft, writing – review & editing. George Kourousias – Data curation, formal analysis, investigation, methodology, software, data curation, validation, visualization, writing – review & editing. Francesco Nespoli – Data curation, investigation, methodology, validation, visualization, writing – review & editing. Paolo Ronchese – Data curation, investigation, methodology, validation, visualization, writing – review & editing. Alessandra Gianoncelli – Conceptualization,

data curation, formal analysis, funding acquisition, investigation, methodology, project administration, resources, software, data curation, validation, visualization, writing – review & editing.

Conflicts of interest

There are no conflicts to declare.

Data availability

The data supporting this article have been included as part of the supplementary information (SI). Supplementary information is available. See DOI: **https://doi.org/10.1039/d5ja00322a**.

Acknowledgements

(1) Co-funding was received from the ZnOrgBat project (no. 23034) under the EIT RawMaterials, part of the Horizon Europe funding scheme. (2) This study was conducted within the MOST–Sustainable Mobility Center activities funded by the European Union Next-GenerationEU programme (PIANO NAZIONALE DI RIPRESA E RESILIENZA (PNRR) – MISSIONE 4 COMPONENTE 2, INVESTIMENTO 1.4 – D.D. 1033 17/06/2022, CN00000023). This manuscript reflects only the authors' views and opinions; neither the European Union nor the European Commission can be considered responsible for them. (3) We acknowledge Elettra Sincrotrone Trieste for providing access to its synchrotron radiation facilities and for financial support under the SUI internal project.

References

1 B. Bozzini and I. Sgura, A Conceptual, Mathematical and Quantitative Reassessment of the Thin-Film Flooded Agglomerate Model for Air Cathodes, *J. Electroanal. Chem.*, 2023, **950**, 117855, DOI: **10.1016/j.jelechem.2023.117855**.

2 Y. Salman, S. Waseem, A. Alleva, P. Banerjee, V. Bonanni, E. Emanuele, R. Ciancio, A. Gianoncelli, G. Kourousias, A. Li Bassi, A. Macrelli, E. Marini and B. Bozzini, synthesis, characterization, functional testing and ageing analysis of bifunctional Zn-air battery GDEs, based on α-MnO_2 nanowires and Ni/NiO nanoparticle electrocatalysts, *Electrochim. Acta*, 2023, **469**, 143246, DOI: **10.1016/j.electacta.2023.143246**.

3 E. A. Carbonio, J.-J. Velasco-Velez, R. Schlögl and A. Knop-Gericke, Perspective—Outlook on Operando Photoelectron and Absorption Spectroscopy to Probe Catalysts at the Solid-Liquid Electrochemical Interface, *J. Electrochem. Soc.*, 2020, **167**, 054509, DOI: **10.1149/1945-7111/ab68d2**.

4 J.-J. Velasco-Vélez, L. J. Falling, D. Bernsmeier, M. J. Sear, P. C. J. Clark, T.-S. Chan, E. Stotz, M. Hävecker, R. Kraehnert, A. Knop-Gericke, C.-H. Chuang, D. E. Starr, M. Favaro and R. V. Mom, A comparative study of electrochemical cells for *in situ* x-ray spectroscopies in the soft and tender x-ray range, *J. Phys. D: Appl. Phys.*, 2021, **54**, 124003, DOI: **10.1088/1361-6463/abd2ed**.

5 B. Bozzini, M. Kazemian Abyaneh, M. Amati, A. Gianoncelli, L. Gregoratti, B. Kaulich and M. Kiskinova, Soft X-ray Imaging and Spectromicroscopy: New Insights in Chemical State and Morphology of the Key Components in Operating Fuel-Cells, *Chem.–Eur. J.*, 2012, **18**, 10196–10210, DOI: **10.1002/chem.201201313**.

6 B. Bozzini, A. Gianoncelli, P. Bocchetta, S. Dal Zilio and G. Kourousias, Fabrication of a Sealed Electrochemical Microcell for *in Situ* Soft X-ray Microspectroscopy and Testing with *in Situ* Co-Polypyrrole Composite Electrodeposition for Pt-Free Oxygen Electrocatalysis, *Anal. Chem.*, 2014, **84**, 664–670, DOI: **10.1021/ac403004v**.

7 V. Berejnov, D. Susac, J. Stumper and A. P. Hitchcock, 3D Chemical Mapping of PEM Fuel Cell Cathodes by Scanning Transmission Soft X-ray Spectrotomography, *ECS Trans.*, 2012, **50**, 361–368, DOI: **10.1149/05002.0361ecst**.

8 B. Bozzini, P. Bocchetta, A. Gianoncelli, C. Mele and M. Kiskinova, Electrodeposition of Co/CoO Nanoparticles Onto Graphene for ORR Electrocatalysis: a Study Based on Micro-X-ray Absorption Spectroscopy and X-ray Fluorescence Mapping, *Acta Chim. Slov.*, 2014, **61**, 263–271.

9 J.-J. Velasco Vélez, Y.-Y. Chin, M.-H. Tsai, O. J. Burton, R. Wang, S. Hofmann, W.-H. Hsu, T. Ohigashi, W.-F. Pong and C.-H. Chuang, Evidence of synergistic electrocatalysis at a cobalt oxide–graphene interface through nanochemical mapping of scanning transmission X-ray microscopy, *Chin. J. Phys.*, 2022, **76**, 135–144, DOI: **10.1016/j.cjph.2021.09.018**.

10 C. Zhang, L. Shahcheraghi, F. Ismail, H. Eraky, H. Yuan, A. P. Hitchcock and D. Higgins, Chemical Structure and Distribution in Nickel−Nitrogen−Carbon Catalysts for CO_2 Electroreduction Identified by Scanning Transmission X-ray Microscopy, *ACS Catal.*, 2022, **12**, 8746–8760, DOI: **10.1021/acscatal.2c01255**.

11 C. O. M. Mariano, J. S. D. Rodriguez, R. H. Clemente, T. Ohigashi, H. Yuzawa, W.-H. Hsu, J. Shiue and C.-H. Chuang, Scanning transmission X-ray microscopy of hydrogen evolution electrocatalysts on reduction graphene oxide membranes, *J. Electron Spectrosc. Relat. Phenom.*, 2023, **265**, 147332, DOI: **10.1016/j.elspec.2023.147332**.

12 W. Zhang, E. Hosono, D. Asakura, H. Yuzawa, T. Ohigashi, M. Kobayashi, H. Kiuchi and Y. Harada, Chemical-state distributions in charged $LiCoO_2$cathode particles visualized by soft X-ray spectromicroscopy, *Sci. Rep.*, 2023, **13**, 4639, DOI: **10.1038/s41598-023-30673-1**.

13 S. D. S. Fitch, G. E. Moehl, N. Meddings, S. Fop, S. Soulé, T.-L. Lee, M. Kazemian, N. Garcia-Araez and A. L. Hector, Combined Electrochemical, XPS, and STXM Study of Lithium Nitride as a Protective Coating for Lithium Metal and Lithium–Sulfur Batteries, *ACS Appl. Mater. Interfaces*, 2023, **15**, 39198–39210, DOI: **10.1021/acsami.3c04897**.

14 B. Bozzini, A. Alleva, V. Bonanni, R. Ciancio, G. Kourousias, F. Guzzi, P. Rajak and A. Gianoncelli, Degradation of α-MnO_2 in Zn-air battery gas-diffusion electrodes: an investigation based on chemical-state mapping, *Electrochim. Acta*, 2024, **513**, 145534, DOI: **10.1016/j.electacta.2024.145534**.

15 C. Zhang, J. Chen, H. Yuan, J. Wang, T. Sun, D. Higgins and A. P. Hitchcock, Atomically dispersed Ni-N-C

electrocatalysts, studied by Ni L-edge spectro-ptychography, *J. Electron Spectrosc. Relat. Phenom.*, 2023, **266**, 147364, DOI: 10.1016/j.elspec.2023.147364.

16 B. Bozzini, G. Kourousias, D. E. Bedolla and A. Gianoncelli, Chemical-state evolution of Ni in Mn-Ni/polypyrrole nanocomposites under bifunctional air electrode conditions, investigated by quasi-in situ multi-scale soft X-ray absorption spectroscopy, *Mater. Today Energy*, 2017, **6**, 154e163, DOI: 10.1016/j.mtener.2017.09.013.

17 B. Bozzini, P. Bocchetta, A. Gianoncelli, G. Kourousias, M. Kiskinova and S. Dal Zilio, In situ soft x-ray fluorescence and absorption microspectroscopy: A study of Mn-Co/polypyrrole electrodeposition, *J. Vac. Sci. Technol., A*, 2015, **33**, 031102, DOI: 10.1116/1.4917551.

18 B. Bozzini, P. Bocchetta, G. Kourousias and A. Gianoncelli, Electrodeposition of Mn-Co/Polypyrrole Nanocomposites: An Electrochemical and *In Situ* Soft-X-ray Microspectroscopic Investigation, *Polymers*, 2017, **9**, 17, DOI: 10.3390/polym9010017.

19 J. Tyler Mefford, A. R. Akbashev, M. Kang, C. L. Bentley, W. E. Gent, H. D. Deng, D. H. Alsem, Y.-S. Yu, N. J. Salmon, D. A. Shapiro, P. R. Unwin and W. C. Chueh, Correlative operando microscopy of oxygen evolution electrocatalysts, *Nature*, 2021, **593**, 67–73, DOI: 10.1038/s41586-021-03454-x.

20 C. Zhang, N. Mille, H. Eraky, S. Stanescu, S. Swaraj, R. Belkhou, D. Higgins and A. P. Hitchcock, Copper carbon dioxide reduction electrocatalysts studied by *in situ* soft X-ray spectro-ptychography, *Cell Rep. Phys. Sci.*, 2023, **4**, 101665, DOI: 10.1016/j.xcrp.2023.101665.

21 C. Zhang, H. Eraky, S. Tan, A. Hitchcock and D. Higgins, In Situ Studies of Copper-Based CO_2 Reduction Electrocatalysts by Scanning Transmission Soft X-ray Microscopy, *ACS Nano*, 2023, **17**, 21337–21348, DOI: 10.1021/acsnano.3c05964.

22 A. P. Hitchcock, C. Zhang, H. Eraky and D. Higgins, In Situ Studies of Cu Catalyzed CO_2 Electro-Reduction by Soft X-ray Scanning Transmission X-ray Microscopy and Soft X-ray Spectro-Ptychography, *Microsc. Microanal.*, 2024, **30**(Suppl 1), 1734–1735, DOI: 10.1093/mam/ozae044.855.

23 P. Ingino, H. Eraky, C. Zhang, A. P. Hitchcock and M. Obst, Soft X-ray spectromicroscopic proof of a reversible oxidation/reduction of microbial biofilm structures using a novel microfluidic *in situ* electrochemical device, *Sci. Rep.*, 2024, **14**, 24009, DOI: 10.1038/s41598-024-74768-9.

24 B. Bozzini, G. Kourousias, A. Gianoncelli, M. W. M. Jones, G. Van Riessen and M. Kiskinova, Soft X-ray ptychography as a tool for in operando morphochemicalstudies of electrodeposition processes with nanometric lateral resolution, *J. Electron Spectrosc. Relat. Phenom.*, 2017, **220**, 147–155, DOI: 10.1016/j.elspec.2017.01.004.

25 N. Ohmer, B. Fenk, D. Samuelis, C.-C. Chen, J. Maier, M. Weigand, E. Goering and G. Schütz, Phase evolution in single-crystalline $LiFePO_4$followed by *in situ* scanning X-ray microscopy of a micrometre-sized battery, *Nat. Commun.*, 2015, **6**, 6045, DOI: 10.1038/ncomms7045.

26 J. Lim, Y. Li, D. H. Alsem, H. So, S. C. Lee, P. Bai, D. A. Cogswell, X. Liu, N. Jin, Y.-s. Yu, N. J. Salmon, D. A. Shapiro, M. Z. Bazant, T. Tyliszczak and W. C. Chueh, Origin and hysteresis of lithium compositional spatiodynamics within battery primary particles, *Science*, 2016, **353**, 6299, DOI: 10.1126/science.aaf4914.

27 H. Zhao, H. D. Deng, A. E. Cohen, J. Lim, Y. Li, D. Fraggedakis, B. Jiang, B. D. Storey, W. C. Chueh, R. D. Braatz and M. Z. Bazant, Learning heterogeneous reaction kinetics from X-ray videos pixel by pixel, *Nature*, 2023, **621**, 289–294, DOI: 10.1038/s41586-023-06393-x.

28 K. Kinose, T. Suzuki, K. Kakinuma, M. Uchida, A. Iiyama and S. Tsushima, Soft X-ray Imaging of Polymer Electrolyte Fuel Cells Using Different Support Materials for Catalyst Layers, *ECS Trans.*, 2021, **104**, 185–190, DOI: 10.1149/10408.0185ecst.

29 R. M. Arán-Ais, R. Rizo, M. Plodinec, P. Grosse, G. Algara-Siller, T. Lunkenbein, S. W. Chee, K. Dembélé and B. Roldan Cuenya, Imaging electrochemically synthesized Cu_2O cubes and their morphological evolution under conditions relevant to CO_2 electroreduction, *Nat. Commun.*, 2020, **11**, 3489, DOI: 10.1038/s41467-020-17220-6.

30 Ts. Tarnev, S. Cychy, C. Andronescu, M. Muhler, W. Schuhmann and Y.-T. Chen, A Universal Nano-capillary Based Method of Catalyst Immobilization for Liquid-Cell Transmission Electron Microscopy, *Angew. Chem., Int. Ed.*, 2020, **59**, 5586–5590, DOI: 10.1002/anie.201916419.

31 N. A. Krans, N. Ahmad, D. Alloyeau, K. P. de Jong and J. Zečević, Attachment of iron oxide nanoparticles to carbon nanofibers studied by *in situ* liquid phase transmission electron microscopy, *Micron*, 2019, **117**, 40–46, DOI: 10.1016/j.micron.2018.10.009.

32 N. Ortiz Peña, D. Ihiawakrim, M. Han, B. Lassalle-Kaiser, S. Carenco, C. Sanchez, C. Laberty-Robert, D. Portehault and O. Ersen, Morphological and Structural Evolution of Co_3O_4 Nanoparticles Revealed by *in Situ* Electrochemical Transmission Electron Microscopy during Electrocatalytic Water Oxidation, *ACS Nano*, 2019, **13**, 11372–11381, DOI: 10.1021/acsnano.9b04745.

33 G. Zhao, Y. Yao, W. Lu, G. Liu, X. Guo, A. Tricoli and Y. Zhu, Direct Observation of Oxygen Evolution and Surface Restructuring on Mn_2O_3 Nanocatalysts Using *In Situ* and *Ex Situ* Transmission Electron Microscopy, *Nano Lett.*, 2021, **21**, 7012–7020, DOI: 10.1021/acs.nanolett.1c02378.

34 Y. Yang, S. Louisia, S. Yu, J. Jin, I. Roh, C. Chen, M. V. Fonseca Guzman, J. Feijóo, P.-C. Chen, H. Wang, Ch. J. Pollock, X. Huang, Y.-T. Shao, C. Wang, D. A. Muller, H. D. Abruña and P. Yang, Operando studies reveal active Cu nanograins for CO_2 electroreduction, *Nature*, 2023, **614**, 262–271, DOI: 10.1038/s41586-022-05540-0.

35 Y. Yang, C. Shi, J. Feijóo, J. Jin, C. Chen, Y. Han and P. Yang, Dynamic Evolution of Copper Nanowires during CO_2 Reduction Probed by *Operando* Electrochemical 4D-STEM and X-ray Spectroscopy, *J. Am. Chem. Soc.*, 2024, **146**, 23398–23405, DOI: 10.1021/jacs.4c06480.

36 A. Impagnatiello, C. Ferreira Cerqueira, P.-E. Coulon, A. Morin, S. Escribano, L. Guetaz, M.-C. Clochard and G. Rizza, Degradation Mechanisms of Supported Pt

Nanocatalysts in Proton Exchange Membrane Fuel Cells: An Operando Study through Liquid Cell Transmission Electron Microscopy, *ACS Appl. Energy Mater.*, 2020, **3**, 2360–2371, DOI: **10.1021/acsaem.9b02000**.

37 S. Brimaud, E. Marini, M. Liebert, F. Rossi, D. Oliveira De Souza, P. Baumli, G. Aquilanti, F. Regnet, I. Lüdeking, B. Bozzini and L. Jörissen, Mapping of the degradation processes at bifunctional O_2 gas diffusion electrode for aqueous alkaline metal-air batteries, *J. Power Sources*, 2022, **546**, 231879, DOI: **10.1016/j.jpowsour.2022.231879**.

38 E. Marini, D. Oliveira De Souza, G. Aquilanti, M. Liebert, F. Rossi and B. Bozzini, In Operando XAS of a Bifunctional Gas Diffusion Electrode for Zn-Air Batteries under Realistic Application Conditions, *Appl. Sci.*, 2021, **11**, 11672, DOI: **10.3390/app112411672**.

39 F. Rossi, E. Marini, M. Boniardi, A. Casaroli, A. Li Bassi, A. Macrelli, C. Mele and B. Bozzini, What happens to MnO_2 when it comes in contact with Zn^{2+}? An electrochemical study in aid of Zn/MnO_2-based rechargeable batteries, *Energy Technol.*, 2022, 2200084, DOI: **10.1002/ente.202200084**.

40 A. Gianoncelli, G. Kourousias, L. Merolle, M. Altissimo and A. Bianco, Current status of the TwinMic beamline at Elettra: a soft X-ray transmission and emission microscopy station, *J. Synchrotron Radiat.*, 2016, **23**, 1526–1537, DOI: **10.1107/S1600577516014405**.

41 A. Gianoncelli, G. R. Morrison, B. Kaulich, D. Bacescu and J. Kovac, Scanning transmission x-ray microscopy with a configurable detector, *Appl. Phys. Lett.*, 2006, **89**, 251117, DOI: **10.1063/1.2422908**.